

Journal Pre-proof

Prominent role of volcanism in Common Era climate variability and human history

Ulf Büntgen, Dominique Arseneault, Étienne Boucher, Olga V. Churakova, (Sidorova), Fabio Gennaretti, Alan Crivellaro, Malcolm K. Hughes, Alexander V. Kirdyanov, Lara Klippel, Paul J. Krusic, Hans W. Linderholm, Fredrik C. Ljungqvist, Josef Ludescher, Michael McCormick, Vladimir S. Myglan, Kurt Nicolussi, Alma Piermattei, Clive Oppenheimer, Frederick Reinig, Michael Sigl, Eugene A. Vaganov, Jan Esper



PII: S1125-7865(20)30096-5

DOI: <https://doi.org/10.1016/j.dendro.2020.125757>

Reference: DENDRO 125757

To appear in: *Dendrochronologia*

Received Date: 13 March 2020

Revised Date: 19 August 2020

Accepted Date: 27 August 2020

Please cite this article as: Büntgen U, Arseneault D, Boucher É, Churakova, (Sidorova) OV, Gennaretti F, Crivellaro A, Hughes MK, Kirdyanov AV, Klippel L, Krusic PJ, Linderholm HW, Ljungqvist FC, Ludescher J, McCormick M, Myglan VS, Nicolussi K, Piermattei A, Oppenheimer C, Reinig F, Sigl M, Vaganov EA, Esper J, Prominent role of volcanism in Common Era climate variability and human history, *Dendrochronologia* (2020), doi: <https://doi.org/10.1016/j.dendro.2020.125757>

This is a PDF file of an article that has undergone enhancements after acceptance, such as the addition of a cover page and metadata, and formatting for readability, but it is not yet the definitive version of record. This version will undergo additional copyediting, typesetting and review before it is published in its final form, but we are providing this version to give early visibility of the article. Please note that, during the production process, errors may be discovered which could affect the content, and all legal disclaimers that apply to the journal pertain.

© 2020 Published by Elsevier.

Prominent role of volcanism in Common Era climate variability and human history

Ulf Büntgen^{1,2,3,4*}, Dominique Arseneault⁵, Étienne Boucher⁶, Olga V. Churakova (Sidorova)^{2,7,8}, Fabio Gennaretti⁹, Alan Crivellaro¹, Malcolm K. Hughes¹⁰, Alexander V. Kirilyanov^{7,11}, Lara Klippel¹², Paul J. Krusic^{1,13}, Hans W. Linderholm¹⁴, Fredrik C. Ljungqvist^{15,16,17}, Josef Ludescher¹⁸, Michael McCormick^{19,20}, Vladimir S. Myglan²¹, Kurt Nicolussi²², Alma Piermattei¹, Clive Oppenheimer¹, Frederick Reinig²³, Michael Sigl²⁴, Eugene A. Vaganov^{7,11}, Jan Esper²³

¹Department of Geography, University of Cambridge, Cambridge CB2 3EN, UK. ²Swiss Federal Research Institute (WSL), 8903 Birmensdorf, Switzerland. ³Global Change Research Centre (CzechGlobe), 603 00 Brno, Czech Republic. ⁴Department of Geography, Faculty of Science, Masaryk University, 613 00 Brno, Czech Republic. ⁵Department of Biology, Chemistry and Geography, University of Québec, Rimouski QC G5L 3A1, Canada. ⁶Department of Geography, University of Québec, Montréal H2X 3R9, Canada. ⁷Institute of Ecology and Geography, Siberian Federal University, 660041 Krasnoyarsk, Russia. ⁸Institute of Humanities, Siberian Federal University, Krasnoyarsk, 660041, Russia. ⁹Forest Research Institute, University of Québec, Abitibi-Témiscamingue, Rouyn-Noranda J9X 5E4, Canada. ¹⁰Laboratory of Tree-Ring Research, University of Arizona, Tucson, AZ 85721, USA. ¹¹Sukachev Institute of Forest SB RAS, Krasnoyarsk, 660036, Russia. ¹²Department of Geography, Justus Liebig University, 35390 Giessen, Germany. ¹³Department of Physical Geography, Stockholm University, 10691 Stockholm, Sweden. ¹⁴Regional Climate Group, Department of Earth Sciences, University of Gothenburg, 40530 Gothenburg, Sweden. ¹⁵Department of History, Stockholm University, 10691 Stockholm, Sweden. ¹⁶Bolin Centre for Climate Research, Stockholm University, 10691 Stockholm, Sweden. ¹⁷Swedish Collegium for Advanced Study, 15238 Uppsala, Sweden. ¹⁸Potsdam Institute for Climate Impact Research (PIK), 14473 Potsdam, Germany. ¹⁹Initiative for the Science of the Human Past at Harvard, Department of History, Harvard University, Cambridge, MA 02138, USA. ²⁰Max Planck–Harvard Research Centre for Archaeoscience of the Ancient Mediterranean, Harvard University, Cambridge, MA 02138, USA. ²¹Institute of Humanities, Siberian Federal University, Krasnoyarsk, 660041, Russia. ²²Department of Geography, University of Innsbruck, 6020 Innsbruck, Austria. ²³Department of Geography, Johannes Gutenberg University, 55099 Mainz, Germany, ²⁴Climate and Environmental Physics (CEP), Physics Institute & Oeschger Centre for Climate Change Research (OCCR), University of Bern, 3012 Bern, Switzerland. *Corresponding author: ulf.buentgen@geog.cam.ac.uk and buentgen@wsl.ch

Keywords: Climate reconstruction; Dendroclimatology; Human history; Northern Hemisphere; tree-ring width; Volcanic eruptions

Abstract

Climate reconstructions for the whole of the Common Era are compromised by the paucity of annually-resolved and absolutely-dated proxy records prior to medieval times. Where reconstructions are based on combinations of different climate archive types of varying spatiotemporal resolution, dating uncertainty, record length and predictive skill, it is challenging to estimate past amplitude ranges, disentangle the relative roles of natural and anthropogenic forcing, and probe deeper interrelationships between climate variability and human history. Here, we compile and analyse updated versions of all the existing summer temperature sensitive tree-ring width chronologies from the Northern Hemisphere that span the entire Common Era. We apply a novel ensemble approach to reconstruct extra-tropical summer temperatures from 1–2010 CE, and calculate uncertainties at continental to hemispheric scales. Peak warming in the 280s, 990s and 1020s, when volcanic forcing was low, was comparable to modern conditions until 2010 CE. The lowest June–August temperature anomaly in 536 not only marks the beginning of the coldest decade, but also defines the onset of the Late Antique Little Ice Age (LALIA). While prolonged warmth during Roman and medieval times roughly coincides with the tendency towards societal prosperity across much of the North Atlantic/European sector and East Asia, major episodes of volcanically-forced summer cooling often presaged widespread famines, plague outbreaks and political upheavals. Our study reveals a larger amplitude of spatially synchronized summer temperature variation during the first millennium of the Common Era than previously recognised. Uncertainties associated with the available tree-ring width measurements emphasize the need to develop more and longer chronologies of wood density and cell anatomy from temperature sensitive sites on both hemispheres where living and relict materials are abundant.

1. Introduction

Placing recent global warming in the context of long-term natural climate variability is fundamental to climate model predictions (e.g., Ljungqvist et al., 2019), and remains a major scientific challenge (e.g., Neukom et al., 2019; PAGES2k Consortium, 2013, 2019). Annually-resolved and absolutely-dated temperature reconstructions that continuously cover the past two millennia and reliably and consistently capture the full range of natural and anthropogenic summer temperature variation are restricted to a few sites across the Northern Hemisphere. High-quality temperature reconstructions from the Southern Hemisphere are even more sparse (Mann and Jones, 2003; Neukom and Gergis, 2012). Multi-proxy climate reconstructions that integrate different archive types of varying record lengths and signal-to-noise ratios are generally limited in their ability to consistently represent both annual extremes and long-term trends over the full record extent back in time (Christiansen and Ljungqvist, 2017; Esper and Frank, 2009b; Frank et al., 2007b). The inclusion of lower resolution proxy data, with inherent dating uncertainty or biases, can result in a virtually flat climate history of the first half of the Common Era (Neukom et al., 2019; PAGES2k Consortium, 2019). In turn, artificial variance reduction not only constrains our understanding of the relative contributions of natural and anthropogenic climate forcing factors (e.g., Hegerl et al., 2006), but also hampers proxy-model comparisons and attribution studies (e.g., Hegerl and Zwiers, 2011). Dating uncertainty and variance reduction in regional- to large-scale temperature or precipitation reconstructions also challenge the investigation of direct and indirect interrelationships between climate variability and human history (e.g., Büntgen et al., 2011, 2016; Campbell, 2016; Büntgen and Di Cosmo, 2016; Di Cosmo et al., 2017).

To address some of the methodological and conceptual hurdles associated with the selection, compilation and investigation of proxy data, as well as to capture the full range of past extra-

tropical summer temperature variation from 1–2010 CE, we apply here a novel ensemble climate reconstruction approach on updated tree-ring width (TRW) chronologies from high-elevation/-latitude sites across the Northern Hemisphere. Despite the parameter-specific limitations of TRW, we explore the multi-scalar impacts of volcanic forcing on our new temperature realisations, and examine possible linkages between volcanism and climate. While critical discussion is devoted to reductionist and deterministic perceptions of the volcano-climate-human nexus, we outline the diagnostic value of annually-resolved and absolutely dated temperature reconstructions in historical arguments.

2. Materials and Methods

We compiled and analysed all the existing and available nine high-elevation/-latitude TRW datasets from the Northern Hemisphere that continuously span the Common Era and are considered to reflect a predominant summer temperature signal (Fig. 1a). Updated into the 21st century, these records combine TRW measurements from living and relict material (Supplementary Table S1). The mid-latitude TRW collections from the western United States (GTB and SCO), Austrian Alps (ALP) and Russian Altai (ALT) represent upper treeline pine and larch environments. The collections from Quebec and Labrador (QUL; spruce), northern Scandinavia (NSC; pine), and northern Siberia (YAM, TAI and NYA; larch) represent northern boreal forest sites. The number of contributing core or disc samples per dataset ranges from 224–2725 series (SCO to QUL), and the majority of TRW measurements was derived from dry-dead snags and subfossil wood remains (i.e., there is a much larger proportion of relict versus living trees). For each of the nine regional datasets, neither the number of TRW series, nor the mean segment length and the mean series age are stable over time (Supplementary Figs. S1–9). All the

Eurasian datasets share a robust common signal over the past two millennia (Supplementary Fig. S10). Annual dating precision of the individual chronologies is independently confirmed by detection of the 774 CE cosmogenic spike in the Earth's atmospheric radiocarbon (^{14}C) concentration (Büntgen et al., 2018).

For each of the nine individual TRW datasets (Fig. 1, Table S1), we developed an ensemble of 16 chronologies based on slightly different Regional Curve Standardization treatments (RCS; Esper et al., 2003; Büntgen et al., 2012). These realisations include varying degrees of filtering of the regional curve (i.e., secondary smoothing of the RC), in combination with variance stabilization, temporal data splitting and index calculation (i.e., ratios or residuals after power transformation) (Cook and Peters, 1997). Moreover, we used both the Standard (STD) and Arstan (ARS) chronology outputs from the latest version of the ARSTAN software (Cook et al., 2017), with the later generally containing less first-order autocorrelation (Cook, 1985). Each of these chronology development techniques was applied on all TRW series per site (all), as well as separately on the living and relict series per site (liv/rel). The resulting RCS chronology versions of the split datasets were merged at equal weight when sample size exceeded 20 series (Büntgen et al., 2011). All the above described combinations of chronology development resulted in a total of 16 slightly different realisations, herein referred to as ensemble members (see Supplementary information for details). Calculating the median of the 16 ensemble members further stabilized the variance of the resulting regional timeseries over the past two millennia (Frank et al., 2007b). The minimum and maximum ensemble values of each year were considered as methodological chronology error limits (Büntgen et al., 2012). We applied this rather simple but efficient ensemble approach because there is no, universally accepted, objective criterion for selecting a single best chronology version. While accepting some degree of disadvantage for some of the sites (i.e., not

always the optimal site chronology), we are convinced that our ensemble approach will ultimately result in sufficient advantages at larger scales (i.e., chronology consistency across the network).

Characterized by long-term persistence (Supplementary Figs. S11–12), each ensemble median exhibits interannual to multi-centennial variability and stable variance through time (Supplementary Fig. S13). The nine regional ensemble medians were correlated against current-year, average June, July or August instrumental temperatures over 1950–2002 CE (Fig. 1). Monthly temperature data were extracted and averaged from the nearest $0.5^\circ \times 0.5^\circ$ CRU TS4.03 (Jones et al., 2012) and $1.0^\circ \times 1.0^\circ$ Berkeley (Rhode et al., 2013) grid cells (Fig. 1). Proxy-target correlations were restricted to the post-World War II period for which the gridded climate indices in all regions are based on a markedly expanded and improved network of meteorological station readings (see Figure 3 in Frank et al., 2007a), and for which each of the individual TRW chronologies is composed of hundreds of TRW samples (Table S1). Data from the latest CRU and Berkeley versions were averaged because they are nearly identical ($r > 0.98$), and there is neither a statistical nor methodological and conceptual justification to prioritize one over the other. Proxy-target correlation coefficients > 0.4 are highly significant after correction for lag-1 autocorrelation ($p < 0.01$). Likely affected by unprecedented anthropogenic drought stress during the past decades (Williams et al., 2020), the two mid-latitude TRW ensemble medians from the Great Basin (GTB; Salzer and Kipfmüller, 2005) and the Southern Colorado Plateau (SCO; Salzer et al., 2014) in the western United States (Fig. 1), do not contain a sufficiently strong temperature signal between 1950 and present. All of the remaining seven ensemble medians (QUL, NSC, ALP, YAM, TAI, ALT, NYA), however, reveal significant positive correlation coefficients ($r > 0.4$; $p < 0.01$) with current-year, average June, July or August temperatures over the 1950–2002 CE period of proxy-target overlap (Fig. 1b). We find the TRW measurements from the Austrian Alps (ALP) are a very

good summer temperature proxy for much of central Europe and parts of the Mediterranean basin, followed by strong relationships between tree growth and summer temperature over inner Eurasia (ALT) and north-central Siberia (YAM and TAI). In these cases, significant positive correlation coefficients ($r > 0.6$; $p < 0.001$) almost entirely resemble the spatial extent obtained from a simple instrumental target-to-target comparison (Fig. 1c). The TRW ensemble medians from Quebec and Labrador (QUL), northern Scandinavia and northern Yakutia (NSC and NYA) are somehow less dependent on warm-season temperature variations after 1950 CE, and synoptically much more constrained.

The seven TRW ensemble medians that exhibit highly significant correlation coefficients with regional June, July or August temperatures were scaled against their best summer season temperature targets using the mean of the nearest CRU and Berkeley grid points (Jones et al., 2012; Rhode et al., 2013). Scaling instead of regression was used to avoid artificial variance reduction (Esper et al., 2005). After scaling at the regional-scale, the median of the six European and Russian ensemble medians was used to reconstruct Eurasian (EA) summer (June–August; JJA) temperatures from 1–2010 CE (i.e., the common period of all remaining regional ensemble medians). After adding the Canadian predictor (QUL), the median of all seven TRW ensemble medians was used to reconstruct summer temperatures over the extended Eurasian/North Atlantic sector (EA+). Restricted to the extra-tropics $>30^{\circ}\text{N}$, both the EA (10°W to 180°E) and EA+ (180°W to 180°E) reconstructions are accompanied by accumulated error bars (Fig. 2). We considered uncertainty estimates from the regional TRW chronologies (using the minimum and maximum values per year from each of the 16 ensemble members), as well as the Root Mean Squared Error (RMSE) from scaling against the gridded regional summer temperatures (Büntgen et al., 2012). We then used the latest generation of tree ring-based, large-scale summer temperature

reconstructions (Schneider et al., 2015; Stoffel et al., 2015; Wilson et al., 2016), as well as the multi-proxy PAGES2k Consortium 2019 global temperature reconstruction (Neukom et al., 2019; PAGES2k Consortium, 2019) for purposes of comparison. All timeseries were rescaled against mean 30–70°N extra-tropical landmass JJA temperature anomalies based on the 1961–90 climatology. The rescaled data were further processed with a 30-year cubic smoothing spline to best visualise their decadal and lower frequency variability.

To estimate the strength of the long-term persistence in both the regional- and large-scale data, we applied the detrended fluctuation analysis (DFA2) (Kantelhardt et al., 2001) and the wavelet analysis (WT2) (Eichner et al., 2003; Koscielny-Bunde et al., 1998; Pelletier and Turcotte, 1997). Both methods have the advantage of not being severely affected by linear deterministic trends in the records. Additionally, the DFA2 can estimate the long-term persistence of much shorter records than other methods are able to. However, DFA2 requires records should be at least about 400 data points long for a reliable estimation of long-term persistence (see Supplementary information for details). It should be noted that the autocorrelation function $C(s) \propto (1-\gamma)s^{-\gamma}$ and power spectral density $S(f) \sim f^{-(1-\gamma)}$ in long-term temperature data decay by power-laws (Eichner et al., 2003; Koscielny-Bunde et al., 1998; Pelletier and Turcotte, 1997). However, both functions exhibit strong finite-size effects and only enable a reliable estimation of the long-term persistence in records with data lengths N well above 10^3 (Lennartz and Bunde, 2009).

3. Results and Discussion

3.1 Temperature history

Total sample size of the EA and EA+ reconstruction is 6767 and 9492 series, respectively (Fig. 1d). Annual sample replication of the EA and EA+ reconstruction ranges from 85–2667 and from

87–2908 series, respectively. With 722 and 857 individual TRW series on average, the EA and EA+ records are well-replicated over most of the past two millennia. DFA2 reveals less long-term persistence in the EA and EA+ compilations (Supplementary Figs. S15–16), as compared to most of the regional ensemble medians. However, the final large-scale temperature reconstructions and their corresponding uncertainty ranges are still arguably biased towards the ‘red’ end of the power spectrum, a condition indicative of TRW (Franke et al., 2013), as opposed to maximum latewood density (MXD) that is generally less affected by biological memory (Büntgen et al., 2006; Esper et al., 2016; Frank et al., 2007a). We must emphasize that the amount of biological memory in TRW chronologies is a possible disadvantage of this parameter over MXD (Björklund et al., 2019). TRW is particularly limited when reconstructing the amplitude and duration of climatic extremes (Ljungqvist et al., 2020). Regrettably, only one MXD chronology that spans the past 2000 years has so far been developed for northern Scandinavia (Esper et al., 2012, 2014). More such data, especially but not exclusively from North America, are needed to improve our understanding of past temperature changes (St. George and Esper, 2019). Along these lines, we advocate the exploration and application of new wood anatomical parameters (Büntgen, 2019). In addition to MXD, we consider Blue Rings particularly skilful to improve the dating accuracy of past volcanic eruptions (Piermattei et al., 2015). In contrast to TRW (Frank et al., 2007; Franke et al., 2013), Blue Rings are not affected by biological memory and have the ability to capture severe ephemeral summer cooling (see also Figure 6b). High-resolution, cell-based anatomical parameters are therefore expected to help unravelling possible short-term associations between volcanism, weather and society that operate on sub-seasonal time-scales (Battipaglia et al., 2010; Brázdil et al., 2005), and are not captured by TRW and MXD.

Due to substantial data overlap and considering some degree of TRW-specific uncertainty, the EA and EA+ reconstructions exhibit nearly identical interannual to multi-centennial variability over the period 1–2010 CE, ($r = 0.94$) (Fig. 2; Supplementary Fig. S14). The EA and EA+ reconstructions correlate at 0.38 and 0.45 with JJA instrumental data over the 1901–2010 full period of overlap ($p < 0.05$), respectively. When independently calculated over two equally long early/late split periods (1901–1955 and 1956–2010), the correlation coefficients change to 0.66 and 0.34 for the EA+ and 0.70 and 0.22 for the EA records. After 40-year smoothing (Fig. 2), the EA+ and EA reconstructions correlate 0.75 and 0.52 with their instrumental targets (1901–2010). The correlation coefficients increase to 0.96 and 0.87 for the EA+ and 0.99 and 0.72 for the EA when using the early/late split periods, respectively. Since both reconstructions fail in reproducing the most recent temperature increase, they provide new large-scale evidence for the ‘Divergence Problem’ in dendrochronology (Briffa et al., 1998; D’Arrigo et al., 2008), the idiosyncratic decoupling of predominantly boreal tree growth to rising instrumental summer temperatures since around the 1970s (Esper and Frank, 2009a). Since industrial pollution and associated atmospheric dimming can be considered a possible source for the ‘Divergence Problem’ at the high-northern latitudes, we argue that the Principle of Uniformity as it applies, *sine qua non*, to dendroclimatology and thus to a substantial part of high-resolution paleoclimatology (Büntgen et al., 2008), remains intact.

Coinciding with the onset of the Late Antique Little Ice Age (LALIA; Büntgen et al., 2016), six of the 20 coldest EA+ and EA summers of the past two millennia occurred within a single decade between 536 and 545 CE (Table 1). Another prominent cold summer of the LALIA was reconstructed for 627 (Di Cosmo et al., 2017). The coldest reconstructed summer, relative to the 1961–90 instrumental mean, is 536 CE (-2.02°C and -1.95°C for the EA+ and EA), followed by

1601 for EA+ (-1.81°C) and 1602 for EA (-1.75°C). The two coldest, non-overlapping decades for the EA+ and EA started in 536 (-1.39°C and -1.41°C) and 1812 (-1.28°C and -1.32°C). The two coldest, non-overlapping 20-year intervals for the EA+ and EA started in 536 (-1.18°C and -1.25°C) and 1809 (-1.07°C and -1.06°C). While we have no doubt about the timing of past summer cooling in our reconstructions, accuracy of the temperature amplitude remains somewhat challenging. This limitation, which is likely more pronounced for TRW than MXD, calls for additional wood density and cell anatomy measurements from those temperature sensitive sites – on both hemispheres – where living and relict materials are abundant.

Despite their conservative error estimates that increase back in time, our new reconstructions reveal peak summer warming during Roman and medieval times in the 280s and 990s (Fig. 2), which arguably exceed the reconstructed modern conditions until 2010 CE. The historical TRW-based estimates, however, do not reach the instrumental-based JJA temperatures of the early 21st century (Fig. 2). The four warmest summers between 282 and 287 CE are exceptional departures within a prolonged period of above average temperatures in the 3rd century (Fig. 2; Table 1), presumably reflecting the last part of a Roman Warm Period (RWP). Following the warmest summer in 990 (EA/EA+ anomalies of 1.21/1.22°C), another sequence of three outstandingly warm summers between 1020 and 1031 CE literally indicates the climax of the Medieval Warm Period (MWP). Elevated, TRW-based temperatures since the 1920s characterize the modern warming trend (MWT), with exceptionally hot summers in 1938, 1939, 1942, and 1964 (Hegerl et al., 2018), as well as 2003 (Luterbacher et al., 2004). A slight pause in this warming trend is evident in the first decade of the 21st century (Fyfe et al., 2016). The three warmest, non-overlapping decades in the EA+ reconstruction occurred during pre-industrial times and started in 280, 989 and 256 CE (0.53°C, 0.45°C and 0.39°C, respectively). The three warmest decades in the EA record

started in 1938 (0.42°C), followed by peak warming of 0.41°C and 0.36°C in the RWP and MWP that started in 280 and 981, respectively.

3.2 Volcanic forcing

We find the signature of volcanic forcing (as indicated by ice core data) is imprinted in different statistical properties of both reconstructions. We compared data from four 50-year periods that cover the LALIA and the three most pronounced episodes of the Little Ice Age (LIA1–3) cold phases (mean AC1 =0.49; mean STDEV =0.44) against data from the corresponding three warm intervals of the RWP, MWP and MWT (mean AC1 =0.18; mean STDEV =0.33) (Fig. 3a). The climatic effects of volcanic eruptions are manifest in the reconstructions' higher first-order autocorrelation (memory) and variance (sensitivity). Moreover, volcanic eruptions can synchronize interannual (e.g., Samalas in 1257; Vidal et al., 2016; Guillet et al., 2017) and multi-decadal (e.g., LALIA; Büntgen et al., 2016; Di Cosmo et al., 2017) summer temperature variation over large parts of the Northern Hemisphere extra-tropics.

In contrast, periods of reduced radiative forcing due to a lack of volcanism parallel prolonged warm phases (Fig. 3b), whereas increased volcanic sulphate deposition in Greenland ice cores (Sigl et al., 2015) coincides remarkably well with the ten coldest summers and the five coldest decades in the CE (Table 1). On centennial timescales, we show a significant negative correlation of -0.56 (-0.58) between reconstructed average EA+ (EA) summer temperatures and total Stratospheric Aerosol Optical Depth (SAOD; Fig. 3b). This relation corroborates arguments that the temporal clustering of large volcanic eruptions can lead to long-term cooling associated with the LALIA and LIA1–3. The three warmest, non-overlapping, 100-year intervals of the past two millennia start in 212, 968 and 1911, corresponding with the RWP, MWP and MWT, respectively.

The first two of these intervals appear to coincide with comparatively weak volcanic forcing (Fig. 3), while the last period experienced unprecedented rates of anthropogenic emissions of greenhouse gases. To consider the cumulative effects of clusters of volcanic eruptions, we calculated the accumulated, Northern Hemisphere extra-tropical SAOD, estimated from ice core records (Toohey and Sigl, 2017). The influence of volcanic eruptions during the three warmest centennial periods ranges from 9.5–15.6 SAOD, which is around half of that associated with the three coldest 100-year intervals when SAOD averages range between around 25 and 35 (Fig. 3b). Since our study provides enough evidence to assume that volcanism represents the predominant control on Northern Hemisphere extra-tropical summer temperature variability during the past two millennia, we argue for a limited influence of both solar irradiance (Steinhilber et al., 2009) and orbital changes (Esper et al., 2012). This hypothesis is supported by the suggestion that the presence of stratospheric volcanic aerosols may alter deposition rates of cosmogenic beryllium (^{10}Be) (Baroni et al., 2011, 2019), which is considered a proxy for past changes in solar activity.

3.3. Amplitude preservation

Compared with state-of-the-art tree ring-based (i.e., using TRW, MXD or a combination thereof), large-scale temperature reconstructions spanning the past 1200–1500 years (Schneider et al., 2015; Stoffel et al., 2015; Wilson et al., 2016), our new reconstructions not only extend further back in time (Fig. 4), but also contain more mid- to low-frequency variability. The overall larger amplitude likely results from a constant number of tree-ring predictors that continuously cover the Common Era. Interestingly, proxy and model evidence independently suggest that data from a few well-selected locations can reflect large-scale climate dynamics surprisingly well (Cook et al., 2004; Jaume-Santero et al., 2020). Compared with the latest generation of PAGES2k products that

include a selection of 257, out of a total of 692 proxy records (Neukom et al., 2019; PAGES2k Consortium, 2019), the herein developed and compiled tree ring-only realisations exhibit more variability (Fig. 4). The initial PAGES2k database contains information from trees (415), ice cores (49), lake and marine sediments (42 and 58), corals (96), historical sources (15), sclerosponges (8), speleothems (4), boreholes (3), bivalves (1), and a hybrid tree/borehole (1), distributed across 648 locations on all continents and major oceans (PAGES2k Consortium, 2017). The apparent amplitude reduction in the PAGES2k record is most striking for the first half of the Common Era (Figs. 4, 5; Supplementary Fig. S17), when the response to volcanic forcing is further diminished (Fig. 6a). Acknowledging some degree of biological memory in TRW, post-eruptive summer cooling of $\sim 0.4^{\circ}\text{C}$ persists for nearly ten years in the EA/EA+ reconstructions (Supplementary Tables S3–4). While the mean negative forcing from our selected volcanic eruptions slightly increases between 100 and 1200 CE, the cooling response of PAGES2k is reduced by 33% (Fig. 6a). Likewise, our EA/EA+ reconstructions exhibit substantially more pre-medieval low-frequency variability compared to the latest PAGES2k product(s), including evidence for the RWP and LALIA (Figs. 4, 5). Based on our new reconstructions, the mid-6th century exhibits the most severe and spatially best synchronized cold spell of the past two millennia (Supplementary Fig. S18). The onset of the LALIA is not only reflected in the seven regional ensemble medians but also by the GTB and SCO datasets from the western United States that were excluded from the large-scale reconstructions. The inability of PAGES2k to capture the putative amplitude range of the LALIA likely results from the relatively low contribution of annually-resolved proxies (1/4 of the predictors during the 6th century). Interestingly, temperatures during the boreal summer of 536 CE most likely dropped below a plant physiological threshold of cell wall lignification at high-elevation/-latitude sites (Crivellaro and Büntgen, 2020). The severe growing season cold spell of

536 immediately resulted in a Blue Ring (Fig. 6b), which refers to a layer of less lignified cell walls that remain blue after double staining with Safranin and Astra blue (Piermattei et al., 2015). The wood anatomical characteristics of our larch sample from the Russian Altai (ALT) indicate abrupt ring width depressions in 536 and 537, associated with almost non-lignified latewood cell walls in 536, followed by a slow recovery until around 543 CE. While similar growth responses have been observed at different sites across the Northern Hemisphere (Churakova (Sidorova) et al., 2019; Helama et al., 2019), the volcano responsible for the onset of the LALIA in 536 CE remains under debate (Loveluck et al., 2018; Dull et al., 2019; Toohey et al., 2016).

3.4 Climate and society

Since radiative forcing due to volcanism was generally weaker during much of the RWP and MWP (Fig. 7), the resulting relatively constant summer warmth may have contributed to societal prosperity and political stability in parts of Europe and China (e.g., Büntgen et al., 2011, 2016; McCormick et al., 2012). Episodes of volcanic-induced abrupt summer cooling, however, tend to coincide with periods of conflict and economic decline (e.g., McCormick et al., 2007). Due to possible changes in sea ice extent and ocean current dynamics (e.g., Patterson et al., 2010), higher temperatures in the 880s and 990s likely facilitated settlements of the Norse expansion in Iceland and Greenland (e.g., Vésteinsson et al., 2002), and possibly the eastward spread of the Thule tradition from the Bering Strait to Greenland (e.g., Friesen and Arnold, 2008). The European voyages of discovery in the 1490s, regarded by some as a viable geopolitical foundation for the concept of the Anthropocene (Lewis and Maslin, 2015; Waters et al., 2016), are contemporaneous with the rapid temperature recovery following LIA1. Despite differences in societal resilience, a reflection of diverse political and economic structures in ecologically-varied regions, demographic

contraction has tended to coincide with periods of relative temperature instability, and cooler summers, and almost always following episodes of negative radiative forcing by volcanic aerosols (Figs. 3b, 7). Episodes of extensive human migration and political turmoil across large parts of Eurasia often correspond with periods of generally lower and more variable summer temperatures from the 4th to the 6th century. We speculate these triggered a range of ‘push-pull’ factors that influenced European-wide migration and the polities of the inner Eurasian steppe.

We note further that the onset and establishment of the three most devastating pandemics also coincide with volcanically-forced, abrupt summer cooling in 165, 541 and 1346 CE (Fig. 7). While it is still debated whether the Antonine Plague, frequently identified as smallpox (*Variola major*), killed many people and impacted Roman Egypt after 165 CE (Harper, 2017), repeated outbreaks of the plague bacillus (*Yersinia pestis*) during the Justinianic Pandemic since the mid-6th century and the Black Death since the mid-14th century (Harper, 2017; Schmid et al., 2015) had major societal, political, cultural and religious ramifications (Campbell, 2016). Eurasia’s putative plague-free period between the first and second pandemics generally matches warmer and less variable summer conditions. Moreover, the fall and transformation of the western Roman Empire in 476, the destruction of the Sasanian Empire from 622, the near annihilation of the early Byzantine Empire from around 634, as well as the collapse of the Eastern Türk Empire in 630, the Abbasid Caliphate in 1258, the Anasazi Culture in the 1290s, and the fall of Constantinople in 1453 (and rise of the Ottoman Empire), all coincide with rapid, interannual summer cooling (Fig. 7). One can add to these cases the demise of the Tang, Liao and Ming Dynasties in 907, 1125 and 1644, respectively. The beginning of the Mongol Conquest in 1206 and its large-scale extent until the 1260s, as well as the Manchu Conquest of China (~1580–1650 at the demise of the Ming Dynasty)

– and even Europe’s Thirty Years’ War (1618–1648) – coincide with intervals of anomalous cold summers.

Complementing the discourse on the effects of climate on dearth and pandemic (e.g., Alfani and Ó Gráda, 2017; Slavin, 2016), our work provides examples of how cold summers due to volcanism coincide with famines at different spatiotemporal scales (Fig. 2). For instance, a decade of Eurasian-wide famines from Ireland to China started in 536 CE and was attributed to the compound effects of volcanic forcing (Toohey et al., 2016). One of the worst famines in Japan’s history occurred from 1229–32 CE. Famines across large parts of the Old World were reported around 1258, north of the Alps from 1315–17, and over parts of western Europe in 1346/47. Japan experienced a severe famine in 1460/61, and a particularly widespread European famine occurred from 1590–98. The worst famine in Russia’s history from 1601–03 followed soon thereafter. Famines in Japan and parts of western and central Siberia occurred from 1641–43, and a very extensive European famine occurred in the 1690s. Famines hit western and central Siberia in 1699, and in 1816/17 one of Europe’s last harvest failures triggered waves of emigration to the United States, for instance. Eastern Siberia experienced its last recent famine in 1819.

Though geographically biased towards Eurasia, our examples strongly suggest volcano–climate entanglements can have an adverse impact on world history (Fig. 7). Nevertheless, future efforts to corroborate and expand our findings should involve model simulations of past demography. Moreover, any hypothesis of an underlying nexus between thermal shocks and subsequent plague outbreaks, widespread famines, falling empires, human migrations, and political transformations requires caution (e.g., Haldon et al., 2018; Mordechai et al., 2019; Oppenheimer, 2015). If longer episodes of climatic and environmental stability favoured growing populations and economies (Hsiang et al., 2013), irrespective of absolute temperature levels, it was

environmental instability at interannual to multi-decadal timescales that seemingly had the opposite effect (Büntgen and Di Cosmo, 2016). To overcome reductionist approaches that aim to establish laws of regularity, the diagnostic power of precise climate reconstructions can shine new light into historical periods in which climatic factors may have had an enhanced impact on human events, and identify those in which societal response dampened that impact. In addition to the use of high-resolution paleoclimatic data in historical arguments, the exploration of putative linkages between climate variability and human history demands contributions from different fields of natural and social sciences (Di Cosmo et al., 2017; Büntgen 2019; Guillet et al., 2020), and the humanities, as well as mutual understanding among its practitioners.

4. Conclusions

In exceeding previous work, this study contains at least six aspects that contribute to our understanding of the natural causes and societal consequences of interannual to multi-centennial summer temperature changes in the Common Era: *i)* With a total of 9492 TRW samples from temperature sensitive high-northern/-elevation sites across the extra-tropical Northern Hemisphere, and with end dates of the regional TRW datasets between 2010 and 2017 CE, each of the seven proxy records continuously reaches back to the year 1 CE. *ii)* Reconstructed summer temperatures in the 280s, 990s and 1020s most likely exceeded the tree ring-based modern warming until 2010 CE. *iii)* Compared with previous large-scale temperature reconstructions, our work reveals a much larger amplitude of spatially well-synchronized, pre-industrial summer temperature variability, including strong evidence for the geographical extent of the LALIA. *iv)* If pre-industrial summers during Roman and medieval times, in the relative absence of volcanic forcing, were sometimes as warm as modern ones, the effects of anthropogenic greenhouse gases

could be larger than anticipated. v) While relatively constant warmth during Roman and medieval times, when volcanic forcing was low, tended to coincide with societal prosperity and political stability in Europe and China, conflict and economic decline often occurred during episodes of enhanced volcanically-forced cooling. vi) Our temperature reconstructions provide new insights into historical periods in which climatic extremes, and their associated environmental responses, arguably have had an outsized impact on human events on the scale of world history.

Caution is, however advised as our new reconstructions are equally far away from being perfect as any other previous attempt using TRW, MXD or a combination of different parameters and proxies. We also acknowledge there exists a substantial level of subjectivity inherent to the complex process of climate reconstruction, beginning with data selection and ending with the interpretation of results. Moreover, there is no doubt that more and better regional composite records are needed for the past two millennia and before. By the same token, well-replicated wood density and cell anatomy chronologies should be developed for those temperature sensitive sites where living and relict wood is abundant. In addition to new high-resolution climate proxy data, we urgently need independent evidence of climate forcing factors to improve the next generation of paleoclimate model simulations and gain a deeper mechanistic understanding of the causes and consequences of past climate dynamics at multiple spatiotemporal scales. Last but not least, we are aware of the conceptual challenges and methodological pitfalls associated with interdisciplinary investigations at the interface of climate variability and human history. Likewise, we are convinced that the generation, interpretation and integration of high-resolution proxy archives promises to answer such critical questions as: How have climatic changes and other environmental factors impacted human demographics, settlement, social structure, agriculture, commerce and conflict; and what climate conditions may be conducive to establishing and

sustaining panzootics and pandemics? How did societies respond to diverse and variable climates, and why were some societies more successful than others? What role did past volcanism play in the waxing and waning of major polities and migrations? Although the answers will vary according to the unique and complex historical circumstances of each society, the questions can be asked with greater focus and nuance as ongoing research produces more robust and spatiotemporally refined climate reconstructions.

Acknowledgements

We are thankful to everyone who made the raw tree-ring data available. Bruce Campbell, Nicola Di Cosmo, Rashit Hantemirov, Joe McConnell, Raphael Neukom, Rob Wilson, and two anonymous referees kindly commented on earlier versions of the manuscript. U.B. received funding from SustES – Adaptation strategies for sustainable ecosystem services and food security under adverse environmental conditions (CZ.02.1.01/0.0/0.0/16_019/0000797). F.C.L. was supported by the Swedish Research Council (grant no 2018-01272). J.L. thanks for the support by the East Africa Peru India Climate Capacities (EPICC) project. M. McC. acknowledges support from the Initiative for the Science of the Human Past at Harvard (SoHP). This project is part of the International Climate Initiative (IKI). The Federal Ministry for the Environment, Nature Conservation and Nuclear Safety (BMU) supports this initiative on the basis of a decision adopted by the German Bundestag. R.H. was supported by the Russian Foundation for Basic Research (grant no 18-05-00575), and A.V.K. received funding from the Russian Science Foundation (grant 18-14-00072). M.S. acknowledges funding from the RRC under the European Union's Horizon 2020 research and innovation programme (grant agreement No 820047).

References

- Alfani, G., Ó Gráda, C., 2017. *Famine in European History*. Cambridge University Press.
- Battipaglia, G., Frank, D.C., Büntgen, U., Dobrovolny, P., Brazdil, R., Pfister, C., Esper, J., 2010. Five centuries of Central European temperature extremes reconstructed from tree-ring density and documentary evidence. *Glob. Planet. Change* **72**, 182–191.
- Baroni, M., Bard, E., Petit, J.-R., Magand, O., Bourles, D., 2011. Volcanic and solar activity, and atmospheric circulation influences on cosmogenic ^{10}Be fallout at Vostok and Concordia (Antarctica) over the last 60 years. *Geochim. Cosmochim. Acta* **75**, 7132–7145.
- Baroni, M., Bard, E., Petit, J.-R., Viseur, S., ASTER Team, 2019. Persistent Draining of the Stratospheric ^{10}Be Reservoir After the Samalas Volcanic Eruption (1257 CE). *J. Geophys. Res. Atmos.* **124**, 7082–7097.
- Björklund J., et al., 2019. Scientific merits and analytical challenges of tree-ring densitometry. *Rev. Geophys.* **57**, 1224–1264.
- Brázdil, R., Pfister, C., Wanner, H., von Storch, H., Luterbacher, J., 2015. Historical climatology in Europe – The state of the art *Clim. Change* **70** 363–430.
- Briffa, K.R., Schweingruber, F., Jones, P., Osborn, T.J., Shiyatov, S.G., Vaganov E.A., 1998. Reduced sensitivity of recent tree-growth to temperature at high northern latitudes. *Nature* **391**, 678–682.
- Büntgen, U., Frank, D.C., Nievergelt, D., Esper, J., 2006. Summer temperature variations in the European Alps, AD 755–2004. *J. Clim.* **19**, 5606–5623.
- Büntgen, U., Frank, D.C., Wilson, R., Career, M., Urbinati, C., Esper J., 2008. Testing for tree-ring divergence in the European Alps. *Glob. Change Biol.* **14**, 2443–2453.

- Büntgen, U., Tegel, W., Nicolussi, K., McCormick, M., Frank, D., Trouet, V., Kaplan, J., Herzig, F., Heussner, U., Wanner, H., Luterbacher, J., Esper, J., 2011. 2500 years of European climate variability and human susceptibility. *Science* **331**, 578–582.
- Büntgen, U., Kaczka, R.J., Trnka, M., Rigling, A., 2012. Ensemble estimates reveal a complex hydroclimatic sensitivity of pine growth at Carpathian cliff sites. *Agricult. Forest Meteorol.* **160**, 100–109.
- Büntgen, U., Di Cosmo, N., 2016. Climatic and environmental aspects of the Mongol withdrawal from Hungary in 1242 CE. *Sci. Rep.* **6**, 25606.
- Büntgen, U., Myglan, V.S., Ljungqvist, F.C., McCormick, M., Di Cosmo, N., Sigl, M., Jungclauss, J., Wagner, S., Krusic, P.J., Esper, J., Kaplan, J.O., de Vaan M.A.C., Luterbacher, J., Wacker, L., Tegel, W., Kirilyanov, A.V., 2016. Cooling and societal change during the Late Antique Little Ice Age from 536 to around 660 AD. *Nat. Geosci.* **9**, 231–236.
- Büntgen, U., et al., 2018. Tree rings reveal globally coherent signature of cosmogenic radiocarbon events in 774 and 993 CE. *Nat. Commun.* **9**, 3605.
- Büntgen, U., 2019. Re-thinking the boundaries of dendrochronology. *Dendrochronologia* **53**, 1-4
- Campbell, B.M.S., 2016. *The Great Transition: Climate, Disease and Society in the Late Medieval World*. Cambridge University Press.
- Christiansen, B., Ljungqvist, F.C., 2017. Challenges and perspectives for large-scale temperature reconstructions of the past two millennia. *Rev. Geophys.* **55**, 40–96.
- Churakova (Sidorova), O.V., Fonti, M.V., Saurer, M., Guillet, S., Corona, S., Fonti, P., Myglan, V.S., Kirilyanov, A.V., Naumova, O.V., Ovchinnikov, D.V., Shashkin, A.V., Panyushkina, I.P., Büntgen, U., Hughes, M.K., Vaganov, E.A., Siegwolf, R.T.W., Stoffel, M., 2019.

- Siberian tree-ring and stable isotope proxies as indicators of temperature and moisture changes after major stratospheric volcanic eruptions. *Clim. Past* **15**, 685–700.
- Crivellaro, A., Büntgen, U., 2020. New evidence of thermally-constrained plant cell wall lignification. *Trends Plant Sci.* **24**, 322–324.
- Cook, E.R., 1985. *A time series analysis approach to tree-ring standardization*. PhD dissertation, University of Arizona, Tucson.
- Cook, E., Peters, K., 1997. Calculating unbiased tree-ring indices for the study of climatic and environmental change. *Holocene* **7**, 361–370.
- Cook, E.R., Krusic, P.J., Peters, K., Holmes, R.L., 2017. *Program ARSTAN version48d2: Autoregressive tree-ring standardization program*. Tree-Ring Laboratory of LDEO.
- Cook, E.R., Esper, J., D'Arrigo, R., 2004. Extra-tropical Northern Hemisphere land temperature variability over the past 1000 years. *Quat. Sci. Rev.* **23**, 2063–2074.
- D'Arrigo, R., Wilson, R., Liepert, B., Cherubini, P. 2008. On the 'Divergence Problem' in northern forests: A review of the tree-ring evidence and possible causes. *Glob. Planet. Change* **60**, 289–305.
- Di Cosmo, N., Oppenheimer, C., Büntgen, U., 2017. Interplay of environmental and socio-political factors in the downfall of the Eastern Türk Empire in 630 CE. *Clim. Change* **145**, 383–395.
- Dull, R.A., Southon, J.R., Kutterolf, S., Anchukaitis, K.J., Freundt, A., Wahl, D.B., Sheets, P., Amaroli, P., Hernandez, W., Wiemann, M.C. and Oppenheimer, C., 2019. Radiocarbon and geologic evidence reveal Ilopango volcano as source of the colossal 'mystery' eruption of 539/40 CE. *Quat. Sci. Rev.* **222**, 105855.

- Eichner, J., Koscielny-Bunde, E., Bunde, A., Havlin, S., Schellnhuber, H.J., 2003. Power-law persistence and trends in the atmosphere: A detailed study of long temperature record. *Phys. Rev.* **68**, 046133.
- Esper, J., Cook, E.R., Krusic, P.J., Peters, K., Schweingruber, F.H., 2003. Tests of the RCS method for preserving low-frequency variability in long tree-ring chronologies. *Tree-Ring Res.* **59**, 81–98.
- Esper, J., Frank, D.C., Wilson, R.J.S., Briffa, K.R., 2005. Effect of scaling and regression on reconstructed temperature amplitude for the past millennium. *Geophys. Res. Lett.* **32**, L07711.
- Esper, J., Frank, D., 2009a. Divergence pitfalls in tree-ring research. *Clim. Change* **94**, 261–266.
- Esper, J., Frank, D., 2009b. The IPCC on a heterogeneous Medieval Warm Period. *Clim. Change* **94**, 267–273.
- Esper, J., Frank, D.C., Timonen, M., Zorita, E., Wilson, R.J.S., Luterbacher, J., Holzkämper, S., Nievergelt, D., Verstege, A., Büntgen, U., 2012. Orbital forcing of tree-ring data. *Nat. Clim. Change* **2**, 862–866.
- Esper, J., Dũthorn, E., Krusic, P.J., Timonen, M., Büntgen, U., 2014. Northern European summer temperature variations over the Common Era from integrated tree-ring density records. *J. Quat. Sci.* **29**, 487–494.
- Esper, J., et al., 2016. Ranking of tree-ring based temperature reconstructions of the past millennium. *Quat. Sci. Rev.* **145**, 134–151.
- Frank, D.C., Büntgen, U., Böhm, R., Maugeri, M., Esper, J., 2007a. Warmer early instrumental measurements versus colder reconstructed temperatures: shooting at a moving target. *Quat. Sci. Rev.* **26**, 3298–3310.

- Frank, D., Esper, J., Cook, E.R., 2007b. Adjustment for proxy number and coherence in a large-scale temperature reconstruction. *Geophys. Res. Lett.* **34**, L16709.
- Franke, J., Frank, D., Raible, C.C., Esper, J., Brönnimann, S., 2013. Spectral biases in tree-ring climate proxies. *Nat. Clim. Change* **3**, 360–364.
- Friesen, T.M., Arnold, C.D., 2008. The Timing of the Thule Migration: New Dates from the Western Canadian Arctic. *American Antiquity* **73**, 527–538.
- Fyfe, J.C., Meehl, G.A., England, M.H., Mann, M. E., Santer, B.D., Flato, G.M., Hawkins, E., Gillett, N.P., Xie, S.-P., Kosaka, Y., Swart, N.C., 2016. Making sense of the early-2000s warming slowdown. *Nat. Clim. Change* **6**, 224–228.
- Guillet, S., Corona, C., Stoffel, M., Khodri, M., Lavigne, F., Ortega, P., Eckert, N., Selenniou, P., Daux, V., Churakova (Sidorova), O., Davi, N., Edouard, J.L., Yong, Z., Luckman, B.H., Myglan, V.S., Guiot, J., Beniston, M., Masson-Delmotte, V., Oppenheimer, C., 2017. Climate response to the Samalas volcanic eruption in 1257 revealed by proxy records. *Nat. Geosci.* **10**, 123–128.
- Guillet, S., Corona, C., Ludlow, F., Oppenheimer, C., Stoffel, M., 2020. Climatic and societal impacts of a “forgotten” cluster of volcanic eruptions in 1108-1110 CE. *Sci. Rep.* **10**, 6715.
- Haldon, J., Mordechai, L., Newfield, T.P., Chase, A.F., Izdebski, A., Guzowski, P., Labuhn, I., Roberts, N., 2018. History meets palaeoscience: Consilience and collaboration in studying past societal responses to environmental change. *Proc. Natl. Acad. Sci. U.S.A.* **115**, 3210–3218.
- Harper, K., 2017. *The Fate of Rome: Climate, disease, and the end of an Empire*. Princeton University Press.

- Hegerl, G.C., Crowley, T.J., Hyde, W.T., Frame, D.J., 2006. Climate sensitivity constrained by temperature reconstructions over the past seven centuries. *Nature* **440**, 1029–1032.
- Hegerl, G.C., Zwiers, F., 2011. Use of models in detection and attribution of climate change. *WIREs Clim. Change* **2**, 570–591.
- Hegerl, G.C., Brönnimann, S., Schurer, A., Cowan, T., 2018. The early 20th century warming: Anomalies, causes, and consequences. *WIREs Clim. Change* **9**, e522.
- Helama, S., Saranpää, P., Pearson, C.L., Arppe, L., Holopainen, J., Mäkinen, H., Mielikäinen, K., Nöjd, P., Sutinen, R., Taavitsainen, J.-P., Timonen, M., Uusitalo, J., Oinonen, J., 2019. Frost rings in 1627 BC and AD 536 in subfossil pinewood from Finnish Lapland. *Quat. Sci. Rev.* **204**, 208–215.
- Hsiang, S.M., Burke, M., Miguel, E., 2013. Quantifying the influence of climate on human conflict. *Science* **341**, 1235367.
- Jaume-Santero, F., Barriopedro, D., García-Herrera, R., Calvo, N., Salcedo-Sanz, S., 2020. Selection of optimal proxy locations for temperature field reconstructions using evolutionary algorithms. *Sci. Rep.* **10**, 7900.
- Jones, P.D., et al., 2012. Hemispheric and large-scale land-surface air temperature variations: An extensive revision and an update to 2010. *J. Geophys. Res.* **117**, D05127.
- Kantelhardt, J.W., Koscielny-Bunde, E., Rego, H.H.A., Havlin, S., Bunde, A., 2001. Detecting long-range correlations with detrended fluctuation analysis. *Physica A* **295**, 441–454.
- Lennartz, S., Bunde, A., 2009. Eliminating finite-size effects and detecting the amount of white noise in short records with long-term memory. *Phys. Rev.* **79**, 066101.
- Lewis, S.L., Maslin, M.A., 2015. Defining the Anthropocene. *Nature* **519**, 171–180.

- Ljungqvist, F.C., Zhang, Q., Brattström, B., Krusic, P.J., Seim, A., Li, Q., Zhang, Q., Moberg, A., 2019. Centennial-scale temperature change in last millennium simulations and proxy-based reconstructions. *J. Clim.* **32**, 2441–2482.
- Ljungqvist, F.C., Thejll, P., Björklund, J., Gunnarson, B.E., Piermattei, A., Rydval, M., Seftigen, K., Støve, B., Büntgen, U. 2020. Assessing non-linearity in European temperature-sensitive tree-ring data. *Dendrochronologia* **59**, 125652.
- Loveluck, C.P., McCormick, M., Spaulding, N.E., Clifford, H., Handley, M.J., Hartman, L., Hoffmann, H., Korotkikh, E.V., Kurbatov, E.V., More, A.F., Sneed, S.B., Mayewski, P.A., 2018. Alpine ice-core evidence for the transformation of the European monetary system, AD 640–670. *Antiquity* **366**, 1571– 585.
- Luterbacher, J., Diertrich, D., Xoplaki, E., Grosjean, M., Wanner, H., 2014. European Seasonal and Annual Temperature Variability, Trends, and Extremes Since 1500. *Science* **303**, 1499–1503.
- Koscielny-Bunde, E., Bunde, A., Havlin, S., Roman, E., Goldreich, Y., Schellnhuber, H.-J., 1998. Indication of a universal persistence law governing atmospheric variability. *Phys. Rev. Lett.* **81**, 729–732.
- Mann, M.E., Jones, P.D., 2003. Global Surface Temperatures over the Past Two Millennia. *Geophys. Res. Lett.* **30**, 1820.
- McCormick, M., Dutton, P.E., Mayewski, P.A., 2007. Volcanoes and the climate forcing of Carolingian Europe, A.D. 750–950. *Speculum* **82**, 865–895.
- McCormick, M., Büntgen, U., Cane, M.A., Cook, E.R., Harper, K., Huybers, P., Litt, T., Manning, S.W., Mayewski, P.A., More, A.F.M., Nicolussi, K., Tegel, W., 2012. Climate Change during

- and after the Roman Empire: Reconstructing the Past from Scientific and Historical Evidence
J. Interdiscip. Hist. **43**, 169–202.
- Mordechai, L., Eisenberg, M., Newfield, T.P., Izdebski, A., Kay, J.E., Poinar, H., 2019. The Justinianic Plague: An inconsequential pandemic? *Proc. Natl. Acad. Sci. U.S.A.* **116**, 25546–25554.
- Neukom, R., Gergis, J., 2012. Southern Hemisphere high-resolution palaeoclimate records of the last 2000 years. *Holocene* **22**, 501–524.
- Neukom, R., Steiger, N., Gómez-Navarro, J.J., Wang, J., Werner, J.P., 2019. No evidence for globally coherent warm and cold periods over the preindustrial Common Era. *Nature* **571**, 550–554.
- Oppenheimer, C., 2015. Eruption politics. *Nat. Geosci.* **8**, 244.
- PAGES2k Consortium, 2013. Continental-scale temperature variability during the past two millennia. *Nat. Geosci.* **6**, 339–346.
- PAGES2k Consortium, 2017. A global multiproxy database for temperature reconstructions of the Common Era. *Sci. Data* **4**, 170088.
- PAGES2k Consortium, 2019. Consistent multidecadal variability in global temperature reconstructions and simulations over the Common Era. *Nat. Geosci.* **12**, 643–649.
- Patterson, W.P., Dietrich, K.A., Holmden, C., Andrews, J.T., 2010. Two millennia of North Atlantic seasonality and implications for Norse colonies. *Proc. Natl. Acad. Sci. U.S.A.* **107**, 5306–5210.
- Pelletier, J.D., Turcotte, D.L., 1997. Long-range persistence in climatological and hydrological time series: analysis, modeling and application to drought hazard assessment. *J. Hydrol.* **203**, 198–208.

- Piermattei, A., Crivellaro, A., Carrer, M., Urbinati, C., 2015. The “blue ring”: anatomy and formation hypothesis of a new tree-ring anomaly in conifers. *Trees Struct. Funct.* **29**, 613–620.
- Rhode, R., Muller, R.A., Jacobsen, R., Muller, E., Perlmutter, S., Rosenfeld, A., Wurtele, J., Groom, D., Wickham, C., 2013. A new estimate of the average earth surface land temperature spanning 1753 to 2011. *Geoinfor. Geostat.: An Overview* **1**, 1.
- Salzer, M.W., Kipfmüller, K.F., 2005. Reconstructed temperature and precipitation on a millennial timescale from tree-rings in the Southern Colorado Plateau, U.S.A. *Clim. Change* **70**, 465–487.
- Salzer, M.W., Bunn, A.G., Graham, N.E., Hughes, M.K., 2014. Five millennia of paleotemperature from tree-rings in the Great Basin, USA. *Clim. Dyn.* **42**, 1517–1526.
- Schmid, B.V., Büntgen, U., Easterday, W.R., Ginzler, C., Walløe, L., Bramanti, B., Stenseth, N.C., 2015. Climate-driven introduction of the Black Death and successive plague reintroductions into Europe. *Proc. Natl. Acad. Sci. U.S.A.* **112**, 3020–3025.
- Schneider, L., Smerdon, J.E., Büntgen, U., Wilson, R.J.S., Myglan, V.S., Kirilyanov, A.V., Esper, J., 2015. Revising midlatitude summer temperatures back to A.D. 600 based on a wood density network. *Geophys. Res. Lett.* **42**, 4556–4562.
- Sigl, M., et al., 2015. Timing and climate forcing of volcanic eruptions for the past 2,500 years. *Nature* **523**, 543–549.
- Slavin, P., 2016. Climate and famines: a historical reassessment. *WIREs Clim. Change* **7**, 433–447.
- Steinhilber, F., Beer, J., Fröhlich, C., 2009. Total solar irradiance during the Holocene. *Geophys. Res. Lett.* **36**, L19704.

- St. George, S., Esper, J., 2019. Concord and discord among Northern Hemisphere paleotemperature reconstructions from tree rings. *Quat. Sci. Rev.* **203**, 278–281.
- Stoffel, M., Khodri, M., Corona, C., Guillet, S., Poulain, V., Bekki, S., Guiot, J., Luckman, B.H., Oppenheimer, C., Beniston, M., Masson-Delmotte, V., 2015. Estimates of volcanic-induced cooling in the Northern Hemisphere over the past 1,500 years. *Nat. Geosci.* **8**, 784–788.
- Toohey, M., Krüger, K., Sigl, M., Stordal, F., Svensen, H., 2016. Climatic and societal impacts of a volcanic double event at the dawn of the Middle Ages. *Clim. Change.* **136**, 401–412.
- Toohey, M., Sigl, M., 2017. Volcanic stratospheric sulfur injections and aerosol optical depth from 500 BCE to 1900 CE. *Earth Syst. Sci. Data* **9**, 809–831.
- Williams, A.P., Cook, E.R., Smerdon, J.E., Cook, B.I., Abatzoglou, J.T., Bolles, K., Baek, S.H., Badger, A.M., Livneh, B. 2020. Large contribution from anthropogenic warming to an emerging North American megadrought. *Science* **368**, 314–318.
- Wilson, R.J.S., et al., 2016. Last millennium northern hemisphere summer temperatures from tree rings: Part I: The long-term context. *Quat. Sci. Rev.* **134**, 1–18.
- Vésteinsson, O., McGovern, T.H., Keller, C., 2002. Enduring impacts: Social and environmental aspects of Viking age settlement in Iceland and Greenland. *Archaeol. Islandica* **2**, 98.
- Vidal, C.M., Métrich, N., Komorowski, J.-C., Pratomo, I., Michel, A., Kartadinata, N., Robert, V., Lavigne, F., 2016. The 1257 Samalas eruption (Lombok, Indonesia): the single greatest stratospheric gas release of the Common Era. *Sci. Rep.* **6**, 34868.

Table 1. Temperature extremes. The ten warmest and coldest reconstructed JJA temperature anomalies (with respect to 1961–90), and their minimum and maximum error range (grey values

refer to extreme years that are only found in one of the two large-scale reconstructions.) The five warmest and coldest, non-overlapping, decades.

| | Year (CE) | JJA Temp (°C) | Error (Min/Max) | | | Year (CE) | JJA Temp (°C) | Error (Min/Max) | |
|--------------------------|-----------|---------------|-----------------|-------|---------------------------|-----------|---------------|-----------------|-------|
| 10 Warmest EA Summers | 990 | 1.21 | 0.35 | 2.10 | 10 Warmest EA+ Summers | 990 | 1.22 | 0.24 | 2.08 |
| | 1942 | 0.82 | -0.08 | 1.85 | | 287 | 0.98 | -0.10 | 1.93 |
| | 1938 | 0.81 | -0.05 | 1.73 | | 282 | 0.91 | -0.19 | 2.15 |
| | 284 | 0.77 | -0.22 | 1.90 | | 284 | 0.89 | -0.19 | 1.93 |
| | 1020 | 0.75 | -0.18 | 1.75 | | 1942 | 0.84 | -0.10 | 1.81 |
| | 287 | 0.75 | -0.25 | 1.65 | | 894 | 0.83 | -0.13 | 1.67 |
| | 1027 | 0.72 | -0.20 | 1.67 | | 840 | 0.81 | 0.07 | 1.40 |
| | 895 | 0.71 | -0.19 | 1.42 | | 759 | 0.81 | 0.06 | 1.37 |
| | 1061 | 0.70 | -0.22 | 1.63 | | 895 | 0.78 | -0.14 | 1.62 |
| | 1964 | 0.70 | -0.16 | 1.62 | | 705 | 0.78 | -0.04 | 1.64 |
| 10 Coldest EA Summers | 537 | -1.50 | -2.28 | -0.91 | 10 Coldest EA+ Summers | 537 | -1.55 | -2.36 | -0.94 |
| | 1813 | -1.53 | -2.28 | -0.79 | | 1819 | -1.59 | -2.32 | -0.80 |
| | 1642 | -1.56 | -2.33 | -0.64 | | 1642 | -1.60 | -2.41 | -0.69 |
| | 1820 | -1.64 | -2.32 | -0.92 | | 1601 | -1.60 | -2.65 | -0.69 |
| | 1819 | -1.65 | -2.32 | -0.94 | | 1820 | -1.61 | -2.33 | -0.79 |
| | 1699 | -1.66 | -2.35 | -0.97 | | 545 | -1.63 | -2.56 | -0.85 |
| | 545 | -1.71 | -2.44 | -0.99 | | 1699 | -1.73 | -2.32 | -0.87 |
| | 543 | -1.71 | -2.44 | -1.03 | | 543 | -1.77 | -2.52 | -1.05 |
| | 1601 | -1.75 | -2.59 | -0.96 | | 1602 | -1.81 | -2.47 | -1.17 |
| | 536 | -1.95 | -2.92 | -1.03 | | 536 | -2.02 | -2.81 | -1.13 |
| 5 Warmest EA Decades | 1938-1947 | 0.42 | -0.35 | 1.32 | 5 Warmest EA+ Decades | 280-289 | 0.53 | -0.30 | 1.35 |
| | 280-289 | 0.41 | -0.46 | 1.21 | | 986-995 | 0.45 | -0.29 | 1.18 |
| | 981-990 | 0.36 | -0.35 | 1.16 | | 256-265 | 0.39 | -0.45 | 1.14 |
| | 256-265 | 0.31 | -0.56 | 1.05 | | 1939-1948 | 0.34 | -0.43 | 1.21 |
| | 1024-1033 | 0.30 | -0.46 | 1.08 | | 836-845 | 0.33 | -0.30 | 0.96 |
| 5 Coldest Decades | 546-555 | -1.09 | -1.76 | -0.41 | 5 Coldest EA+ Decades | 1695-1704 | -1.00 | -1.69 | -0.26 |
| | 800-809 | -1.11 | -1.85 | -0.42 | | 1459-1468 | -1.11 | -1.67 | -0.56 |
| | 1459-1468 | -1.12 | -1.71 | -0.50 | | 1601-1610 | -1.15 | -1.89 | -0.41 |
| | 1812-1821 | -1.32 | -2.00 | -0.63 | | 1812-1821 | -1.28 | -1.97 | -0.53 |
| | 536-545 | -1.41 | -2.18 | -0.74 | | 536-545 | -1.39 | -2.18 | -0.66 |

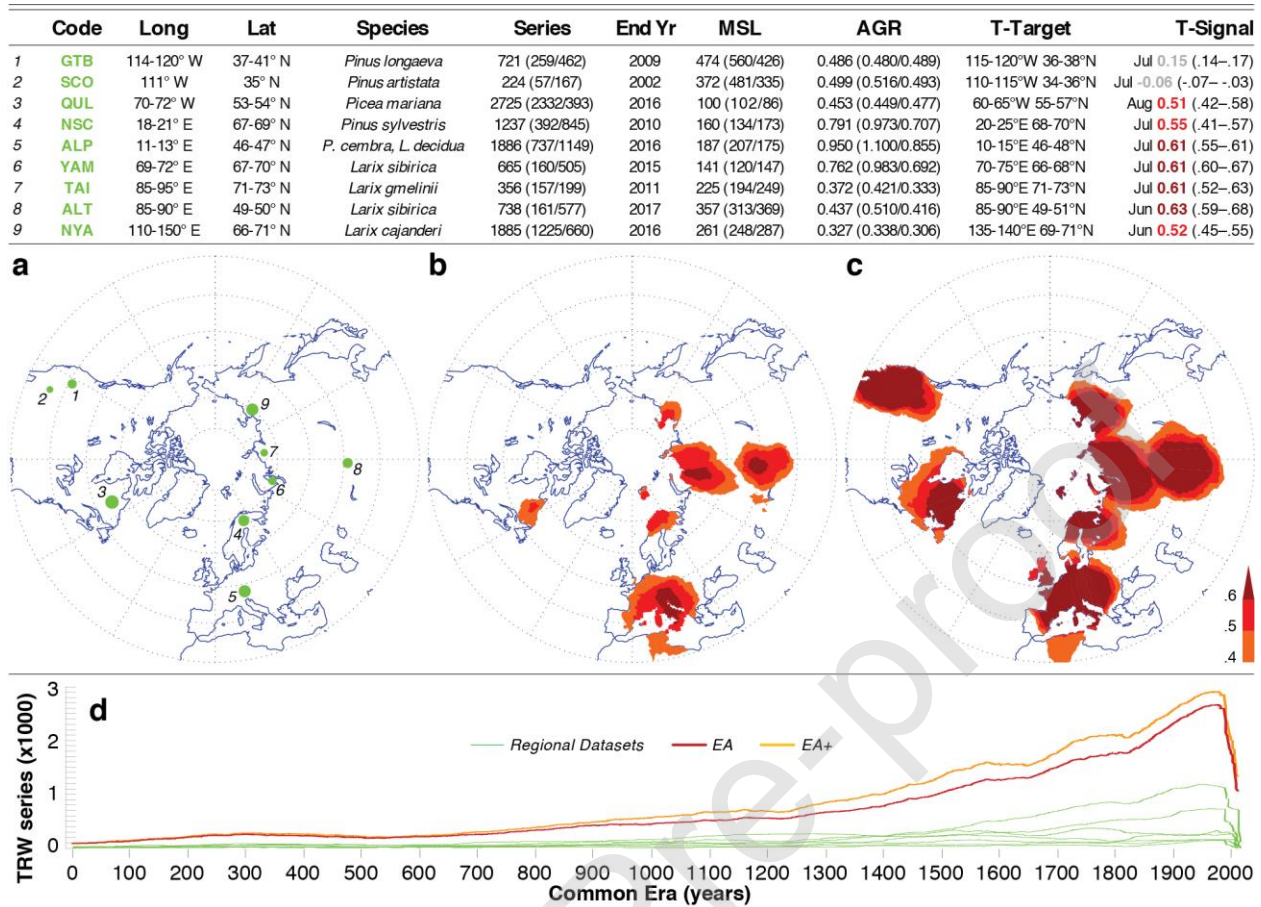


Fig. 1. Tree-ring network. Chronology characteristics of all nine TRW datasets considered in this study (see also Supplementary Table S1). ‘Series’ refers to sample size; ‘MSL’ and ‘AGR’ refer to the mean segment length and average growth rate of all trees in each TRW compilation. Brackets contain information on the proportion of living and relict samples in each collection with 1950 being the threshold year. The spatial domain over which the gridded temperature indices were averaged is presented under ‘T-Target’, and the highest correlations of the individual ensemble medians against mean monthly temperatures are indicated under ‘T-Signal’ (1950–2002 CE), along with the range of correlations from the 16 ensemble members per site. (a) Location of the nine TRW datasets, where the dot size represents sample replication between 224 (SCO) and 2725 (QUL). (b) Spatial field correlation coefficients ($r > 0.4$) of the individual TRW ensemble medians against site-specific gridded monthly summer temperature means ($0.5^\circ \times 0.5^\circ$ CRU TS4.03),

calculated over the extra-tropics $>30^{\circ}\text{N}$ from 1950–2002 CE. (c) As (b) but using the latest version of Berkeley ($1.0^{\circ} \times 1.0^{\circ}$) temperature means (averaged over the tree-ring sites) instead of the TRW proxies (see Supplementary information for details). (d) Temporal changes in sample size of the nine regional TRW datasets and their larger-scale EA and EA+ compilations that contain 6767 and 9492 series, respectively.

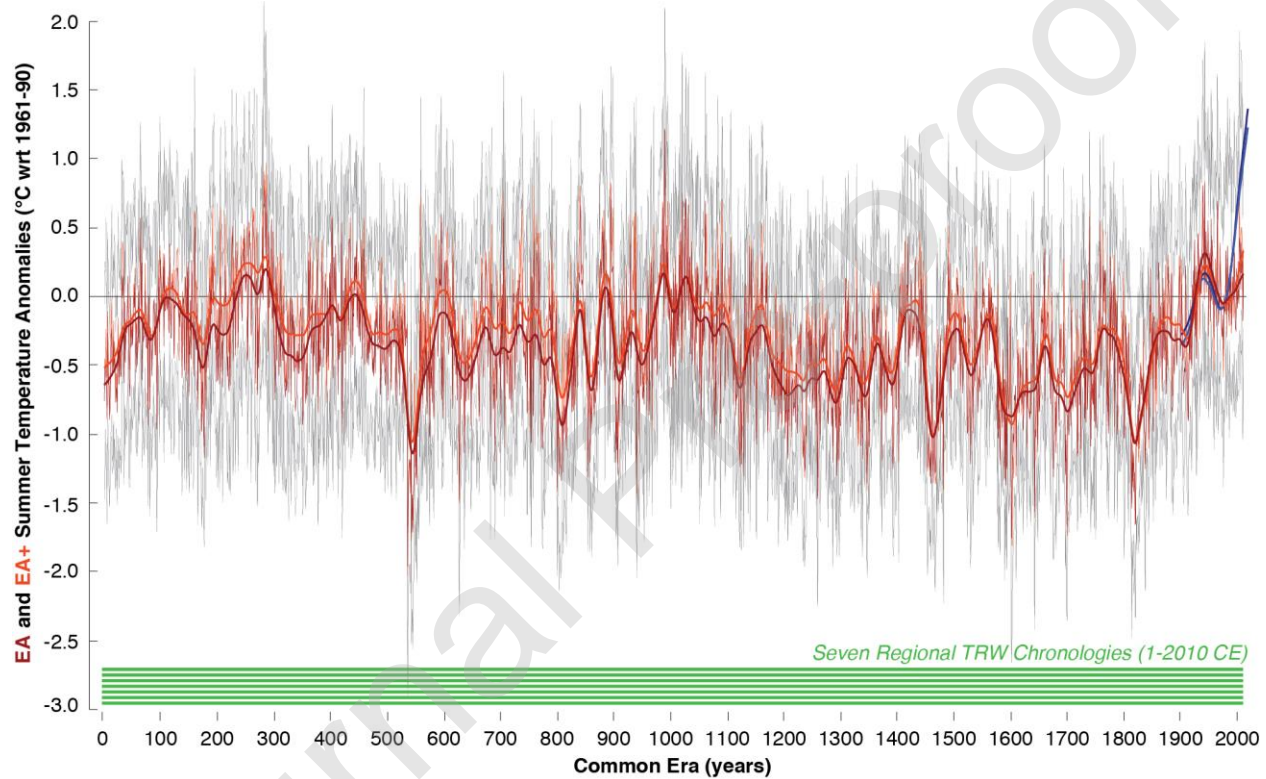


Fig. 2. Temperature reconstruction. The annually-resolved and absolutely-dated, extra-tropical EA and EA+ summer temperatures reconstructions (dark and light red) from 1–2010 CE (based on 6767 and 9492 individual ring width series from living and relict trees). Grey lines refer to the combined uncertainty ranges and the smoothed curves are 40-year low-pass filtered. Blue curves are JJA instrumental temperature means of the EA and EA+ (darker and lighter) from 1901–2018 CE, and green bars refer to the constant number of individual proxy records over time.

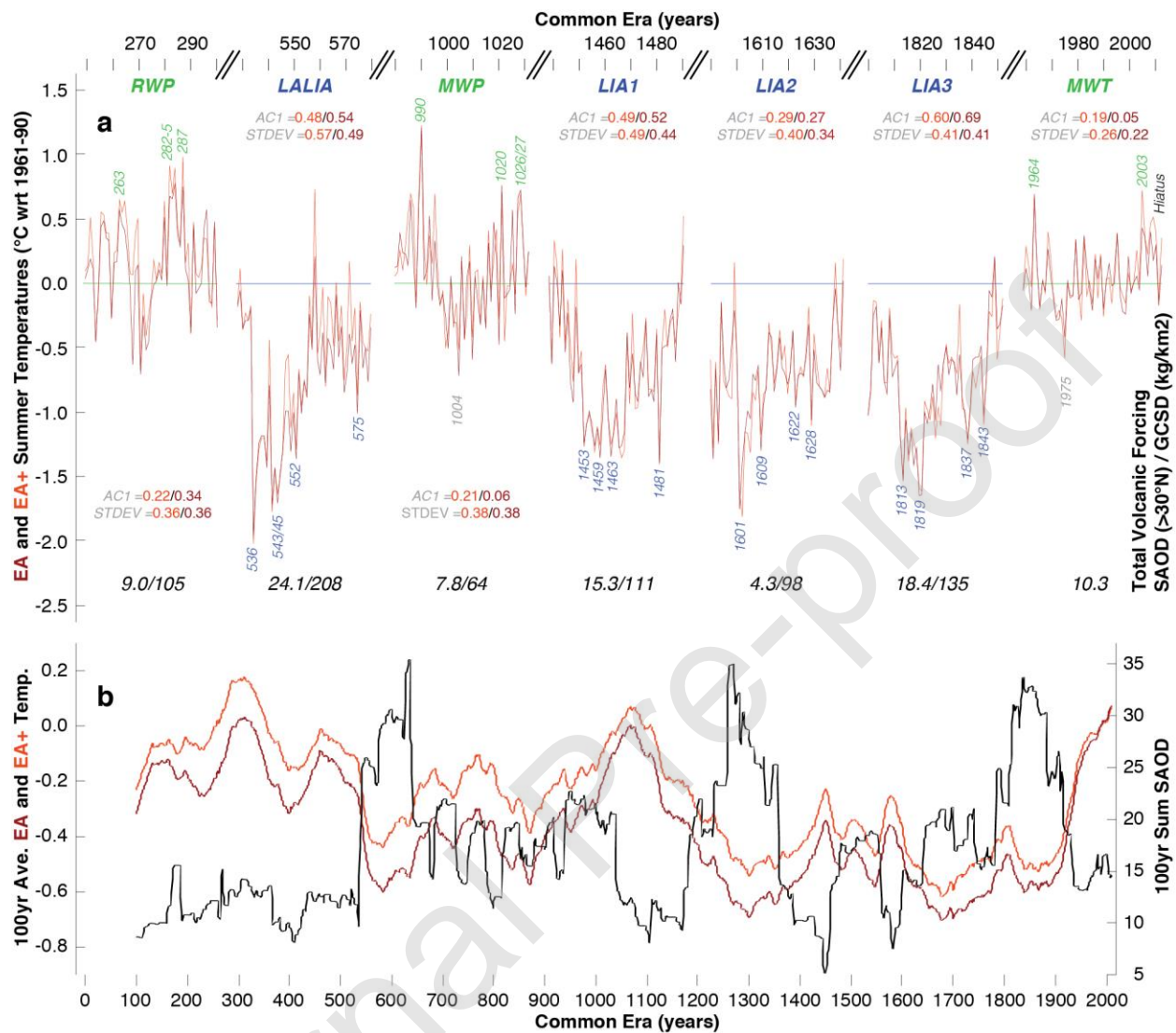


Fig. 3. Temperature extremes. (a) The three warmest (RWP, MWP, MWT) and four coldest (LALIA, LIA1, LIA2, LIA3) 50-year intervals that are well-synchronized over large parts of the Northern Hemisphere extra-tropics (see Fig. 2 and Table 1 for details). First-order autocorrelation (AC1) and standard deviation (STDEV) of the EA and EA+ reconstructions were calculated for each of the seven periods. A proxy for the summed radiative forcing due to volcanism in each of the 50-year periods is provided by the corresponding SAOD and GCSD data (see Supplementary

information for details). **(b)** Comparison between one-tailed, 100-year average EA/EA+ summer temperature anomalies ($^{\circ}\text{C}$ with respect to 1961–90) and one-tailed, 100-year total SAOD data.

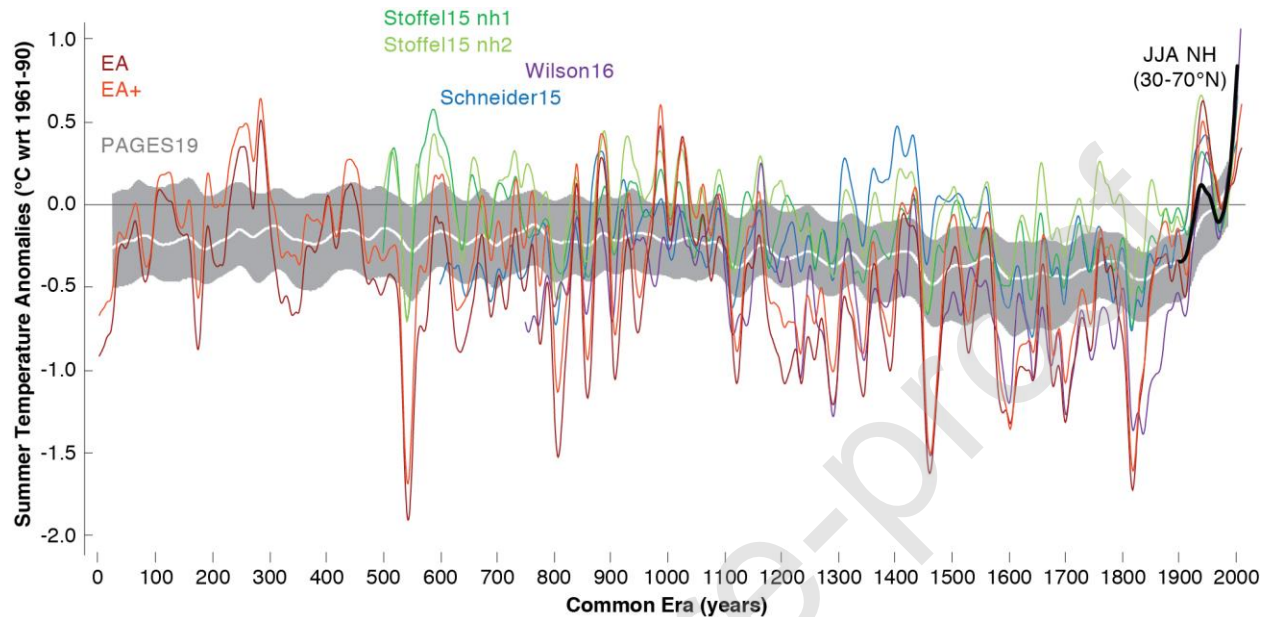


Fig. 4. Large-scale comparison. The EA and EA+ summer temperatures reconstructions together with four tree ring-based, annually-resolved large-scale summer temperature records (Schneider et al., 2015; Stoffel et al., 2015; Wilson et al., 2016). Each timeseries has been rescaled against mean 30–70°N extra-tropical landmass JJA temperature anomalies of 1961–90 (black curve), and was further processed with a 30-year cubic smoothing spline to emphasize decadal and lower frequency behaviour. The rescaled and smoothed tree ring-based summer temperature reconstructions are superimposed to the median and 95% range (2.5th and 97.5th percentiles) of the full 7000-member ensemble across all methods of the latest PAGES2k Consortium 2019 global mean temperature reconstructions (Neukom et al., 2019; PAGES 2k Consortium, 2019).

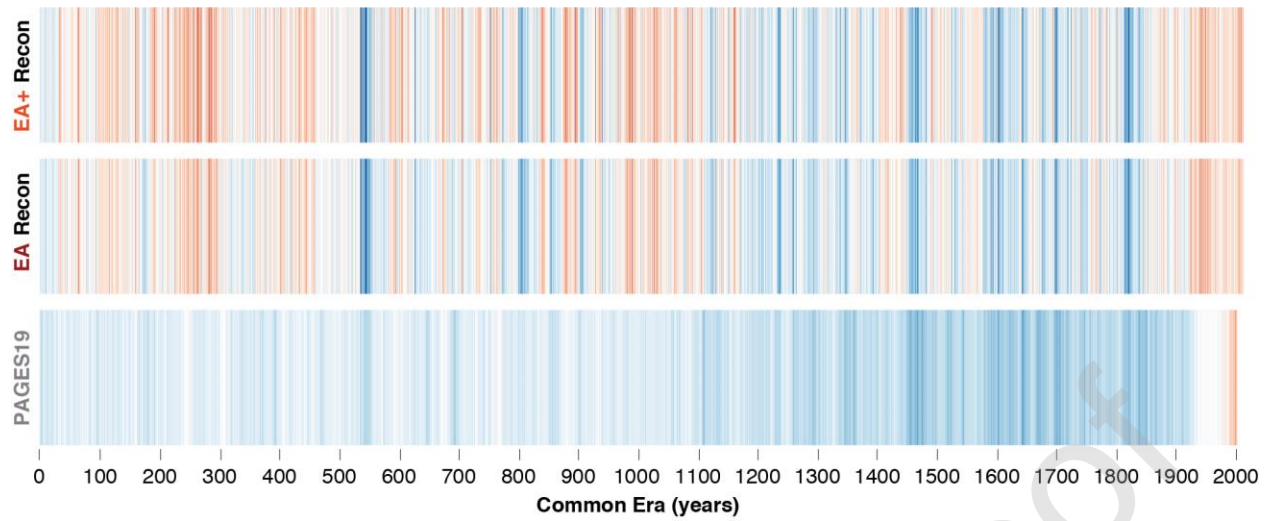


Fig. 5. Temperature stripes. Reconstructed JJA temperatures expressed in 15 different colour stripes from cold to warm (dark blue to dark red). The annual values were scaled to the mean of 1971–2000 and the standard deviation of 1901–2000.

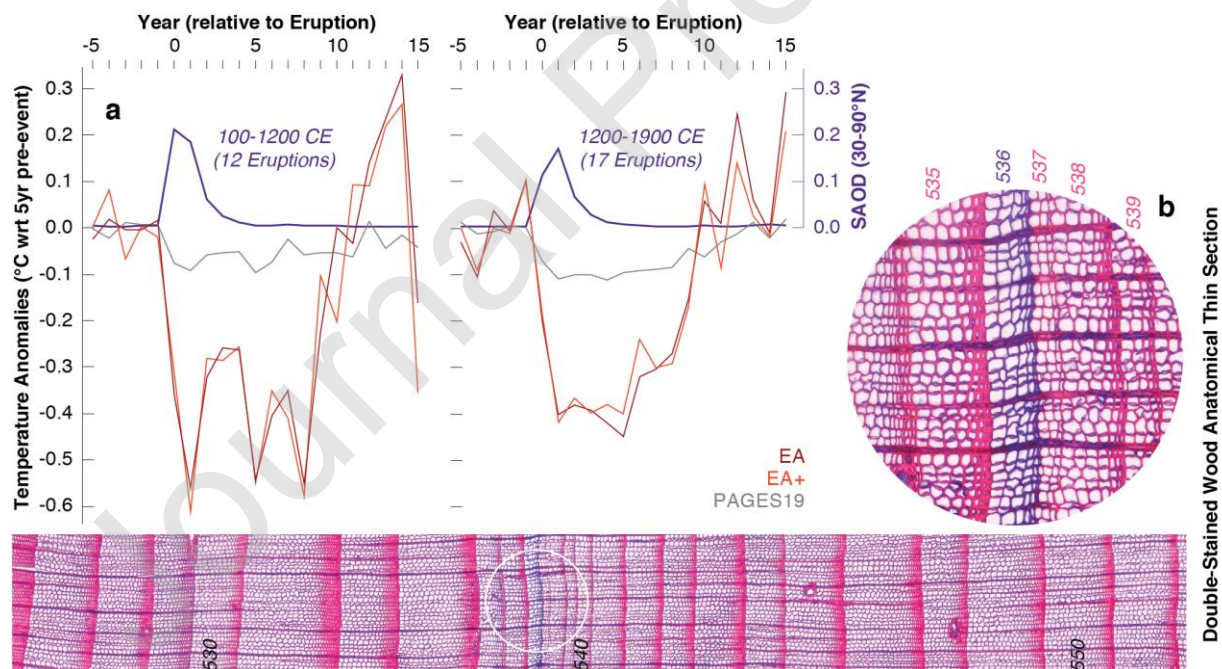


Fig. 6. Volcanic forcing. (a) Superposed composites (i.e., time segments of selected reconstruction periods aligned over 29 eruptions) of volcanic forcing ($SAOD_{30-90^{\circ}N}$; Toohey and Sigl, 2017) and temperature response of our new EA/EA+ reconstructions and the PAGES2k

median of the full 7000-member ensemble to a total of 12 of the strongest individual volcanic forcing events before 1200 (left panel), and 17 of the strongest individual volcanic forcing events between 1200-1900 (Supplementary Table S3). Peak volcanic forcing either appears in year 0 or year 1 after the volcanic eruption depending on the latitude and season. Forcing and response are calculated relative to a pre-event 5-year background period undisturbed by volcanic forcing (e.g., 1804–1808 for the 1809 and 1815 volcanic eruptions, respectively). Data after secondary eruptions (e.g., data from lag +6 years following the 1809 eruption) are removed prior to data aggregation (Supplementary Table S4). (b) Double-stained thin section of a larch disc sample from the upper treeline in the Russian Altai Mountains (ALT) shows a Blue Ring in 536 CE.

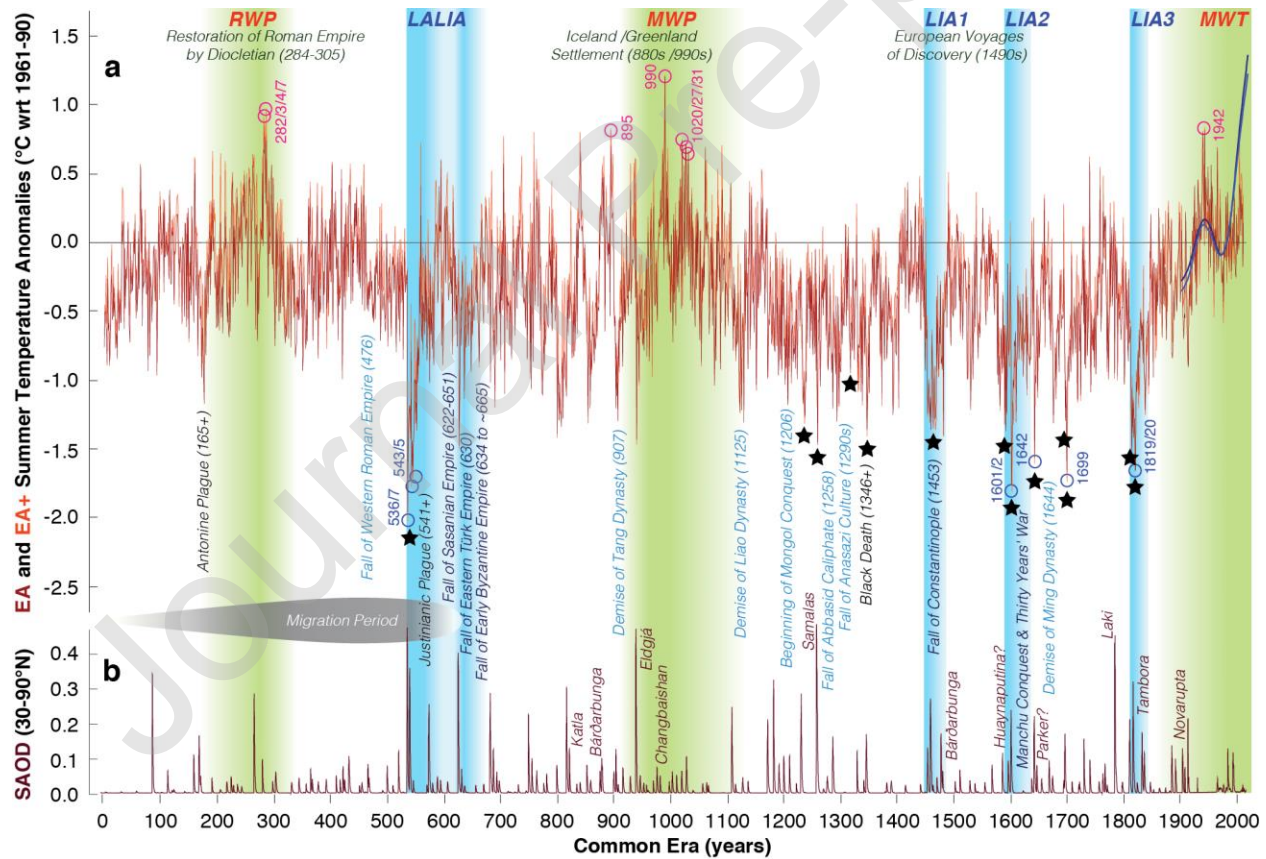


Fig. 7. Volcano-climate-human nexus. (a) Reconstructed summer temperatures and their uncertainties (in light and dark grey, respectively), superimposed on the warmest and coldest periods of the CE (green and blue shadings). The new EA and EA+ JJA reconstructions are shown as temperature anomalies with respect to 1961–90 CE (horizontal line). Pink and blue circles highlight the ten warmest and coldest summers, respectively (see Table 1 for details). While major plague pandemics, political transformations and human occupation and migration are labelled, black stars refer to important famines. (b) Estimated SAOD for 30–90°N with known volcanic eruptions quoted.